JOURNAL OF PROPULSION AND POWER
Vol. 19, No. 1, January–February 2003

Investigation of Instabilities in a Lean, Premixed Step Combustor

Jeffrey M. Cohen,* Brian E. Wake,† and Dochul Choi‡
United Technologies Research Center, East Hartford, Connecticut 06108

A combined experimental and computational characterization of combustion instabilities in a lean, premixed backward-facing step combustor was performed. Specifically, the instabilities of interest were those encountered as the equivalence ratio was reduced to levels approaching the combustor's lean extinction limit. A quasi-one-dimensional unsteady analysis with loss and heat-addition models was developed to simulate combustion instabilities for a premixed step combustor. Experimental results indicated that the magnitude of a longitudinal acoustic disturbance grew with decreasing equivalence ratio, until it eventually triggered a lower-frequency, high-amplitude instability. Numerical results compared with experimental data demonstrated that the analysis can capture the critical frequencies observed in the combustor model. Coupling the heat release with the step flow velocities in the analysis produced an instability at the dominant resonant frequency of the combustor. Experimentally, low-frequency instabilities were visible as a flapping of the flame and increased in severity with decreasing equivalence ratio until they caused combustor blowout.

Nomenclature

A	=	cross-sectional area
a	=	speed of sound
D	=	hydraulic diameter
e	=	internal energy per unit mass
f	=	skin-friction coefficient,
f_l	=	losses caused by blockage and sudden area changes
f_μ	=	skin-friction losses
H	=	enthalpy
h	=	step height [1 in. (2.5 cm)]
$\dot{m}$	=	mass flow rate
n	=	gain for n-τ combustion model
P	=	fluid static pressure
$\dot{q}$	=	heat-release rate
q_n	=	n-τ component of heat release
St	=	Strouhal number, $\omega h/u_{\text{step}}$
T	=	temperature
t	=	time
u	=	flow velocity
x	=	axial distance
γ	=	ratio of specific heats
Δt	=	time step
ζ	=	loss factor
ρ	=	fluid density
τ	=	characteristic time of combustion
ϕ	=	equivalence ratio
ω	=	frequency

Subscripts

s	=	source term
step	=	quantities on top of the step
0	=	total quantities

Received 11 March 1997; revision received 11 October 2002; accepted for publication 14 October 2002.

*Senior Research Engineer, Systems Department, 411 Silver Lane, MS 65; cohenjm@utrc.utc.com.
†Senior Research Engineer, Systems Department, 411 Silver Lane.
‡Fellow, Systems Department, 411 Silver Lane.

Introduction

INCREASED emphasis on reducing the NO_x emissions created by gas turbines has led to the development of lean, premixed combustion systems. For lean mixtures the principal mechanism of NO_x production is primarily a function of local flame temperature and residence time at that temperature. Compared to nonpremixed systems, lean, premixed combustors allow the majority of the fuel to be burned at lower temperatures, thereby producing less NO_x.

A problem inherent to lean combustion systems is related to engine turndown ratio. If a combustor is designed to operate with a lean stoichiometry at high engine power level, it must operate with a very lean stoichiometry at low engine power level. As the power is decreased, combustion instabilities in the system can be observed, indicating that the fuel/air mixture at low power is too lean for the combustor to operate in a stable fashion. These instabilities are often precursors to an incipient blowout of the flame.

Piloting can be used to stabilize the system and prevent this instability from occurring. A pilot flame provides a source of heat in the flame stabilization region, enabling the continuous ignition of fresh reactants. Pilot flames are usually diffusion flames, which, by burning at high flame temperatures, create significant NO_x emissions of their own. It is desirable, then, to reduce the amount of piloting required to stabilize lean, premixed combustion at low engine power levels.

If the nature of the combustion instabilities that precede blowout is understood, it might be possible, through the use of passive design modifications or active control techniques, to reduce the amount of fuel directed to the pilot flame or to eliminate the pilot flame completely. It is the aim of this investigation to characterize these instabilities in a model combustor and to determine, from those data, the mechanisms through which the instabilities are created.

Because of the complexity of the problem being addressed in this study, it was attractive to make simplifications in the geometry of the model combustor relative to the geometry of a real, in-service combustor. Most modern combustors utilize swirling flow through a sudden expansion in order to stabilize a flame. Recirculation regions are created, which return hot products to act as a heat source for the continuous ignition of fresh reactants. Because the effects of swirl on the dynamic nature of the combusting flowfield are not well understood, this study was carried out using a simplified, two-dimensional, rectangular dump combustor. This was embodied by a single-sided sudden expansion in a rectangular duct. This backward-facing step configuration has been studied extensively, both in combusting and cold-flow experiments.[1–6] However, the studies of combustion instabilities have been focused on flashback

phenomena, which occur at high fuel/air ratios far from the lean blowout limit. A schematic of the flowfield is shown in Fig. 1. It reproduces some of the more important characteristics of the flowfield in a real device (recirculation, shear-layer mixing), while eliminating some of the complexity. The present studies were conducted with ambient temperature air at atmospheric pressure.

This study employed complementary computational and experimental methods in order to provide further insight into the problem being studied. In addition, this approach allowed for the development of both analytical and experimental tools that can be used for more complex combustor systems.

Description of the Combustor

The combustor model was divided into three sections, as shown in Fig. 2. The premixing section was designed specifically to provide uniform mixing of natural gas fuel and air. The upstream flange on this section connected directly to the facility airflow plenum.

The fuel delivery system is shown in Fig. 3. In all cases the fuel was natural gas. The fuel flow rate was metered using a choked venturi. Each of the internal manifolds was ovalized [$\frac{3}{4}$-in. (1.9-cm)-diam tube] to reduce its disturbance to the airflow. Choked orifices were located at both ends of both manifolds in order to isolate the majority of the fuel system from combustor pressure variations. Natural gas fuel was injected perpendicular to the oncoming airflow through four arrays of 50 × 0.043-in. (1.1-mm)-diam holes. The size of these holes was determined using jet-penetration guidelines[7,8] to give the most uniform cross-stream coverage. The fuel injection sites were located at the upstream end of the premixing section, which was 24 in. (61 cm) long. The cross-sectional area of the duct was contracted near the end of the premixing section to enhance both flow and mixing uniformity.

The model test section was built using 12 × 4 in. (30.5 × 10 cm) rectangular pipe [0.25 in. (0.64 cm) wall]. The inside of the test section was lined with 0.5-in. (1.3-cm)-thick ceramic insulation. The step was made of stainless steel and was 1 in. high. A 10.0-in. (25.4-cm)-long linear ramp led up to a 3-in. (7.5-cm) flat section approaching the step. This, in combination with a 2-in.-thick piece of honeycomb at the test section inlet, was used to make the approach flow more uniform. The area approaching the step was 17.70 in.^{2} (114 cm^2). The area downstream of the step was 28.36 in.^{2} (183 cm^2). The expansion ratio over the step was 1.6. The test section was equipped with quartz, Schlieren grade windows on either side of the step. The windows were 10.5 × 2.75 in. (26.7 × 7.0 cm) and had a field of view starting 1 in. (2.5 cm) upstream of the step. A spark igniter was inserted through the lower wall of the combustor, mounted flush with the surface.

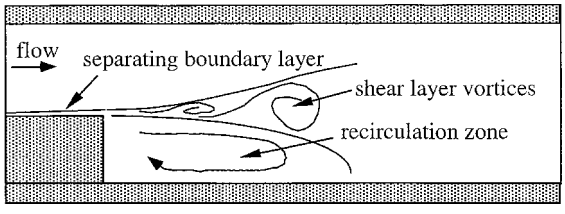

Fig. 1 Schematic of backward-facing-step flowfield.

At a location 18.5 in. (47 cm) downstream of the step, dilution air was introduced through rows of 10 × 0.5-in. (1.3-cm)-diam holes in both the lower and upper walls. These holes were sized to give midspan jet penetration at an airflow rate equal to the main airflow rate in order to form a cold "air curtain" at the exit of the test section. Air was delivered to these holes through two identical manifolds, which were fed through a choked metering orifice. The pressure upstream of the orifice was varied to provide the proper dilution airflow rate. For all tests discussed here, the ratio of the dilution airflow rate to the model airflow rate was 1.0. This flow rate did not enter into the calculation of combustor equivalence ratio.

The exhaust section was equipped with water spray nozzles to cool the exhaust stream leaving the test section. These were located 6.0 in. (15.2 cm) downstream of the dilution air injection. The exhaust section was canted away from the test section so that any excess water ran into the exhaust stack, not into the model. The downstream end of the exhaust section connected directly to the facility exhaust stack through a sudden expansion into a large diameter pipe. The area expansion ratio was approximately 9.0.

Air was delivered to the model using a choked, variable area venturi, fed by a large plenum. The area of the venturi and the pressure in the plenum were adjusted to deliver a known mass flow rate of air into the model. The choke plane of the venturi was located at 6.0 in. (15.2 cm) upstream of the fuel injection manifold. The total length of the model from this choke plane to the sudden expansion at the end of the exhaust section was 87 in. (221 cm).

Part I: Computational Simulation

The objective of the computational work described in this paper was to develop a simplified quasi-one-dimensional Euler analysis that could be used to characterize the primary features of the instability. The analysis must be computationally efficient so that it can be used as a simulator to evaluate active control algorithms. The computational results will be compared with the experimental data to develop and validate the analysis and aid in the interpretation of the experimental data.

Numerical Method

The unsteady quasi-one-dimensional Euler analysis used in this study is a cell-based finite volume technique that uses Roe's upwind-biased differencing scheme.[9] The details of the numerical scheme

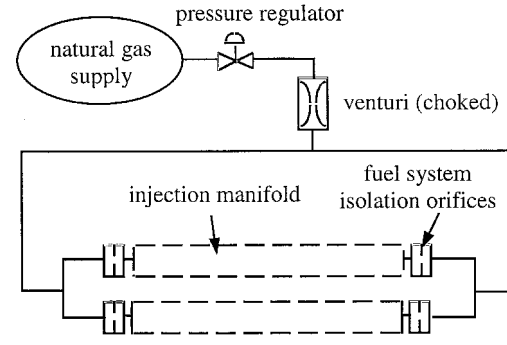

Fig. 3 Schematic illustration of natural gas fuel system.

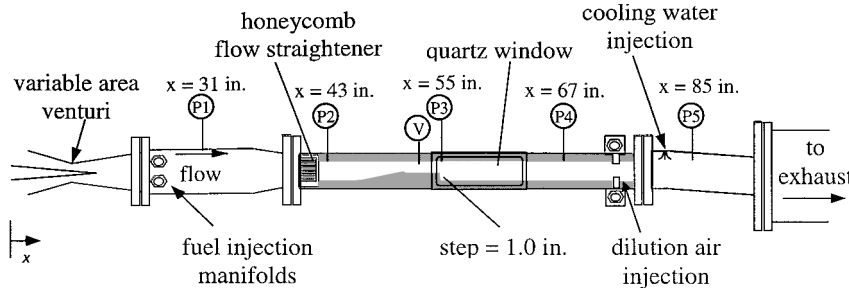

Fig. 2 Schematic illustration of experimental rig.

for the three-dimensional Navier–Stokes equations can be found in other papers.[10–12] Some of the significant features of the scheme are described here.

The unsteady Euler equations were written for a variable-area geometry. Additional source terms were added to model features such as momentum losses and the addition of mass and heat. The equations were nondimensionalized by the inlet total quantities. The reference length was 1 in., and the reference time was the ratio of the reference length and inlet total speed of sound. In nondimensional form the governing equations can be written as

$$\frac{\partial(\rho A)}{\partial t} + \frac{\partial(\rho u A)}{\partial x} = \frac{\partial(\dot{m}_s)}{\partial x} \tag{1}$$

$$\frac{\partial(\rho u A)}{\partial t} + \frac{\partial(\rho u^2 A + P A)}{\partial x} - P\frac{\partial A}{\partial x} = -f_s - f_l \tag{2}$$

$$f_\mu = \frac{1}{2}\rho u^2 A \frac{4f}{D}\,\mathrm{sign}(u) \tag{3}$$

$$f_l = \frac{\partial\left(\frac{1}{2}\rho u^2 A \zeta\right)}{\partial x} \tag{4}$$

$$\frac{\partial(\rho e_0 A)}{\partial t} + \frac{\partial(\rho u H_0 A)}{\partial x} = \frac{\partial(\dot{m} H_0 + \dot{q})_s}{\partial x} \tag{5}$$

where the pressure is given by the equation of state and the total internal energy per unit mass and total enthalpy are given by their definitions:

$$P = (1/\gamma)\rho T \tag{6}$$

$$e_0 = [1/\gamma(\gamma - 1)T] + \tfrac{1}{2}u^2 \tag{7}$$

$$H_0 = [1/(\gamma - 1)]T_0 = [1/(\gamma - 1)]T_0 + \tfrac{1}{2}u^2 \tag{8}$$

The source term in the mass (1) is the summation of the mass addition caused by the injection of dilution air, fuel, and water. The source terms in the momentum (2) are the losses caused by the effects of wall skin friction and other losses such as those caused by sudden area changes. The losses across the honeycomb (flow straightener in Fig. 2) were included by the skin-friction losses. The friction loss factor f was estimated from the hydraulic diameter and the Reynolds number in the different sections of the rig. The pressure loss factor was estimated based on the different area expansion and contraction ratios. The first source term in the energy equation (5) represents the energy flux caused by fluid injection. The second source term in Eq. (5) includes the effect of the heat addition from combustion and the heat absorption from the water evaporation.

Roe's scheme was used to evaluate the inviscid flux terms at the cell-face locations. Third-order accuracy was obtained in the spatial direction by interpolation of the flow characteristic variables to the cell faces.[9] Temporal accuracy was achieved by using Newton subiterations within each time step. At the upstream boundary the total pressure and the total temperature were specified to the inlet plenum conditions of the experiment, and the upstream-running Riemann invariant was extrapolated from the interior of the domain. For the downstream boundary the static pressure was specified. Other quantities were extrapolated from the interior of the domain. The analysis was tested extensively with internal flow model problems. It was found that by using 100 grid nodes and 100 time steps per cycle the propagating pressure waves were captured accurately (less than 0.1% change in amplitude) over the domain of interest. Based on this, the time step was chosen to give 100 time steps per cycle of the highest frequency of interest (130 Hz). This corresponds to a Nyquist frequency of 6.5 kHz for the analytical results, which was more than adequate for comparison to the experimental data.

Numerical Results

The computational domain extended from the plenum to the exhaust exit where the static pressure was atmospheric. The area distribution of the combustor model is shown in Fig. 4a. The choked

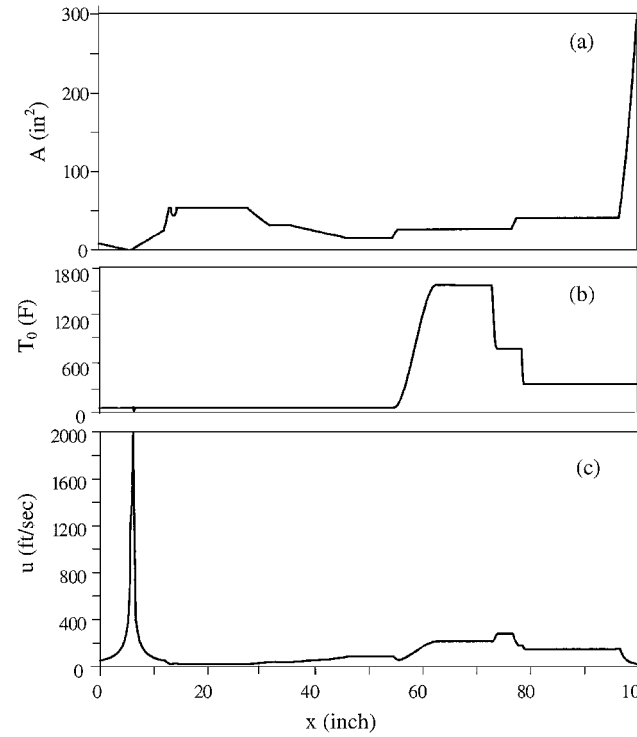

Fig. 4 Distributions of cross-sectional area, total temperature, and velocity in combustor rig.

area in the venturi was 0.8 in.^{2} (5.2 cm^2). At the exit the area was expanded to 290.0 in.^{2} (1871 cm^2). For the calculations presented here 367 grid points were used. The mass flow rate was 0.8 lbm/s (0.36 kg/s), which produced a bulk flow velocity of 87 ft/s (26.5 m/s) on top of the step. A fuel/air equivalence ratio of 0.65 was used, corresponding to the unstable conditions of the experiment. Simple calculations were used to compute a mean heat release using the equivalence ratio and mass flow rate of the air. The resulting temperature was close to the measured flame temperature.

Steady-State Analysis

The calculations were first run in the steady-state mode to compute the initial flowfield. The computed distribution of total temperature is shown in Fig. 4b. The total temperature rise from combustion is evident from $x = 55$ in. (140 cm) at the step to $x = 63$ in. (160 cm). The heat addition for combustion was spread over a distance of 8 in. (20.3 cm) because this was approximately the distance observed in the experiment. The total temperature then drops with the injection of the room-temperature air [$x = 73$ in. (185 cm)] and the water [$x = 78.5$ in. (200 cm)]. The velocity distribution is shown in Fig. 4c. The large rise in the velocity near $x = 60$ in. (152 cm) is caused by the decrease in density caused by the combustion. The velocity increases near $x = 73$ in. (185 cm) as a result of the additional mass of the air injection, even though the flow was cooled at this location. Further downstream the velocity decreases as water is added for cooling, and the area expands.

Unsteady Analysis

To identify the dominant natural acoustic modes for the combustor rig, a random perturbation was added to the mean heat release at every time step. The heat release was then given by

$$\dot{q} = \bar{q} + \Delta q \cdot \mathrm{rand}(-1, 1; \Delta t) + q_n \tag{9}$$

where rand$[-1, +1; \Delta t]$ denotes a random number between -1 and $+1$, selected at a time interval of Δt ($\Delta t = 0.000075$ s for the cases presented here), and $\Delta q = 0.05\bar{q}$. To examine the effect of a simple coupling between the combustion heat release and the step velocity, an n-τ heat-release component was added that was proportional to the fluctuating velocity on top of the step. This velocity on the step

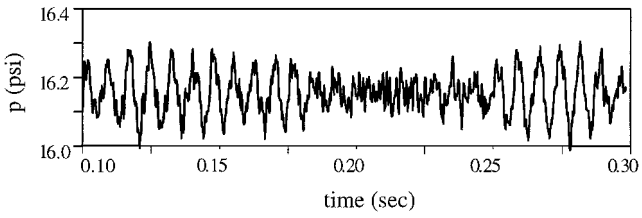

Fig. 5 Time history of pressure fluctuation at $x = 62$ in. (158 cm) with random perturbation of heat release.

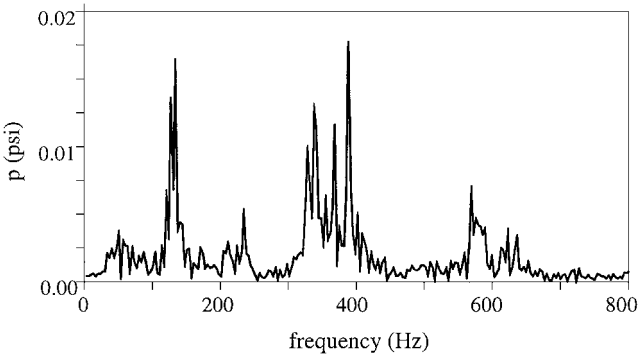

Fig. 6 Frequency spectrum of pressure fluctuation at $x = 12$ in. (30.5 cm) with random perturbation of heat release.

was lagged by the characteristictime τ. Using the n-τ coupling, this component of the heat release then had the form:

$$q_n = [n/(\gamma - 1)]\{[u(t - \tau) - \bar{u}]/\bar{u}\}_{\text{step}} \qquad (10)$$

This component was added to the mean heat release and the random component [Eq. (9)].

The analysis was initially run without the n-τ coupling ($n = 0$). The time history of the pressure in the hot section (P4 in Fig. 2) is shown in Fig. 5. Although the unsteady disturbance was introduced as a 13-kHz random fluctuation, the time history of pressure exhibits noticeable lower-frequency sinusoidal components. A fast Fourier transform (FFT) analysis was performed at several axial locations to identify all important frequencies that were present. In Fig. 6 the spectral content of pressure at the $x = 12$ in. (30.5 cm) location is presented. At this location, the computed dominant frequencies are 127, 386, and 569 Hz. There were two other weaker peaks at 49 and 234 Hz.

These predicted frequencies are fundamental to the combustor and are present in the results without the n-τ coupling. However, the predicted 49-Hz peak is very weak. As will be discussed later in this paper, this frequency is of interest because this mode appeared in the experiment when the combustion was unstable. It cannot be stated, however, that the analysis predicted this mode, a priori, to be potentially unstable. Instead, the analysis was simply used to investigate the 49-Hz mode. Thus, the unstable 49-Hz mode seen in the experiment was not readily anticipated by the analysis.

Mode shapes of the unsteady pressure are shown for several frequencies (49, 127, and 386 Hz) in Fig. 7. In this figure the envelope of the unsteady pressure mode shapes are shown, that is, the unsteady pressure component vs distance at two instants in time. The mode shapes were constructed by forcing the heat release at the specified frequency. The low frequency 49-Hz mode was strongest upstream of the combustor step. This mode was approximately a $\frac{1}{4}$ wave relative to the distance between the venturi and the step. The 127-Hz mode was determined to be approximately a $\frac{3}{4}$ wave relative to the distance between the venturi and the combustor exit (full length), and the 386-Hz mode was about a $2\frac{1}{4}$ wave relative to the full length. All of these mode shapes have antinodal locations just downstream of the venturi and nodal locations at the exit. Upstream of the venturi there were no noticeable pressure oscillation because the flow was choked in the venturi [$x = 5.5$ in. (14 cm)].

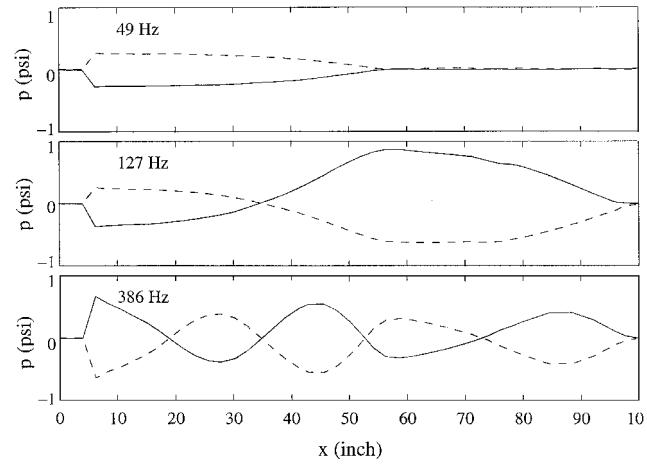

Fig. 7 Distributions of amplitudes of pressure fluctuation for the first three modes.

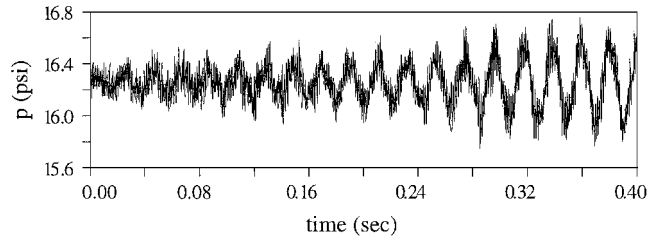

Fig. 8 Pressure fluctuation at $x = 62$ in. (158 cm) with heat release coupled with step velocity ($\tau = 0.015$ s).

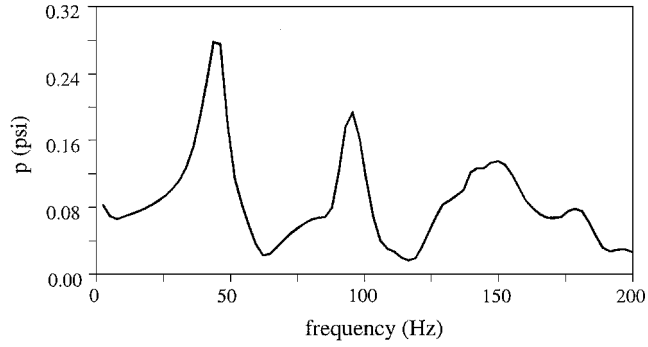

Fig. 9 Frequency spectrum of pressure fluctuation at $x = 62$ in. (158 cm) with heat release coupled with step velocity ($\tau = 0.015$ s).

The pressure time history for the P4 [$x = 62$ in. (158 cm)] location is shown in Fig. 8 for $n = 15$ and $\tau = 0.015$ s. This simple coupling of the heat release with the step velocity produced an amplification in the fluctuations at a frequency near 49 Hz. The n-τ model is an adhoc model, used to represent the coupling between the acoustics and heat release. The time delay and gain are functions of the three-dimensional fluid dynamics and combustion processes and would have to be determined experimentally. For this study the values of the model parameters were adjusted to demonstrate an unstable growth of different modes. The n-τ model did not determine the fundamental acoustic frequencies that were predicted. These frequencies were computed by the analysis without the coupling model. An FFT analysis of the pressure (Fig. 9) reveals that a 98-Hz mode appears as a result of the amplification of the 49-Hz mode.

In the experiment discussed in the next section, large-amplitude unsteadiness occurred at a frequency of 48 Hz. When this occurred, a 96-Hz mode also appeared. The 125-Hz acoustic mode was observed during stable and unstable combustion. To analyze the relationship between the two lower frequency modes numerically, the heat release was perturbed at a frequency of 48 Hz. The FFT analysis of pressure for this case is shown in Fig. 10. The 96-Hz mode was

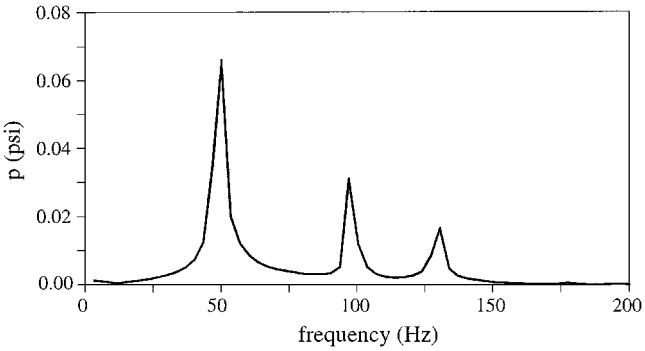

Fig. 10 Frequency spectrum of pressure fluctuation at $x = 62$ in. (158 cm) using 48-Hz perturbation to heat release.

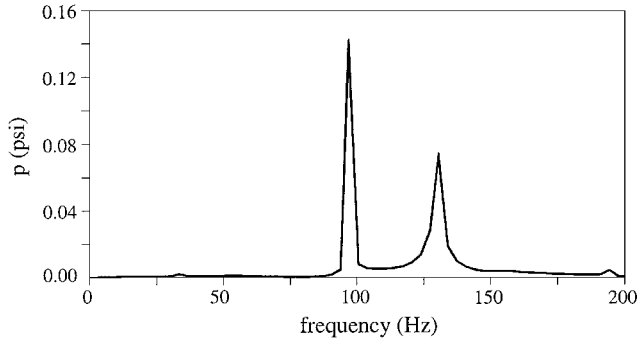

Fig. 11 Frequency spectrum of pressure fluctuation at $x = 62$ in. (158 cm) using 96-Hz perturbation to heat release.

created by the 48-Hz forcing, and the 127-Hz acoustic mode also appeared. Conversely, a 96-Hz perturbation of the heat release was then examined. The FFT analysis of pressure is shown in Fig. 11. For this case the 127-Hz acoustic mode again appears, but the lower frequency 48-Hz mode does not. These results are consistent with the experiment in that the dominant acoustic mode, 127 Hz, was always present, and the 48-Hz mode produced the harmonic at 96 Hz, whereas the 96-Hz forcing did not produce the lower-frequency 48-Hz mode.

Part II: Experiment

Experimental Diagnostics

Combustion instabilities often result from the coupling of acoustic disturbances and fluid flow structure with the heat release in the combustor. The physical variables that best characterize the instability would therefore be those which describe the coupling of the acoustics, heat release, and fluid mechanics. Descriptions of the magnitudes, shapes, and temporal behavior of different acoustic modes can be derived from a series of axially spaced wall/static-pressure measurements. These measurements were simple and reliable and provided data sufficient for direct comparison with computational results.

Static-pressure measurements were made at five axial locations along the centerline of the model (see Fig. 2). The locations were chosen in order to measure the changes imposed on the flow by the different sections of the model. PCB model 103A02 microphones were mounted in water-cooled housings attached directly to the upper wall (opposite the step) of the model. The cavity between the sensor and the inner wall of the model had a constant cross-sectional area and was approximately 0.75 in. (1.9 cm) long.

Data were acquired using a 10-channel, simultaneous sample-hold data system. Analog signals from the sensors were fed into the data system and digitized at a rate of 6.25 kHz. Antialiasing filters, set at 2 kHz, were used on all channels. The data acquisition system recorded 64,000 words of data per data point for each channel. This led to a data record length of approximately 10.5 s. The data were downloaded to an internal hard disk on a dedicated Compaq 386 PC. These files were converted into a binary format compatible with MATLAB® data analysis software, which was used for analysis of the high-response data.

Visualization of the reacting flowfield was accomplished using a focused, single-pass shadowgraph system. A stroboscopic light source (EG&G model 501), with a 1 μs pulse duration, was used to illuminate the combustion zone downstream of the step. The system used F/5 mirrors with 6.0-in. (15.2-cm) apertures to collimate the light and to focus the resulting image. Optical access was through the quartz windows on either side of the combustor. Images were recorded using either a standard VHS video camera (30 frames/s) or a high-speed 16-mm movie camera (1000 frames/s).

Other secondary measurements were made during the course of the experiment. The thickness of the boundary layer approaching the step was measured using a hot-film anemometer to be approximately 0.25 in. (0.64 cm) at a distance 1.0 in. (2.5 cm) upstream of the step. The boundary-layer velocity profile indicated a fully developed turbulent boundary layer. Some measurements of the velocity in the constant-area section approaching the step were made. During unstable operation, however, the hot-film probe was destroyed on a regular basis, and only limited data were acquired under those conditions. The mixedness of the reactants at the dump plane of the combustor was not measured.

Experimental Results and Discussion

For the sake of definition, "stable" operation was characterized by low levels of pressure fluctuation in the combustor, whereas "unstable" combustion was characterized by high levels of pressure fluctuation and flame motion. In this experiment the unstable behavior reached a high-amplitude limit cycle that was capable of causing flame extinction.

Stable Combustion

Tests were conducted over a range of equivalence ratios (ϕ) and airflow rates for which the combustor operated in a stable manner. In general, this corresponded to operating at equivalence ratios above 0.80. Airflow rates ranged between 0.6 lbm/s (0.27 kg/s) and 1.0 lbm/s (0.45 kg/s), corresponding to a one-dimensional velocity range of 65–109 ft/s (19.8–33.2 m/s) in the constant-area section upstream of the step. In these stable combustion tests spectral peaks were observed in the pressure signals at a frequency of 124 Hz, as illustrated in Fig. 12. The mode shape, calculated using the pressure measurement array, indicates that this frequency corresponds to a standing $\frac{3}{4}$ wave mode for the entire system, confirming the predictions presented in the preceding section. Both the velocity and heat-release measurements (not presented here) showed similar behavior.

Unstable Combustion

Combustion instabilities were encountered as the fuel/air ratio of the combustor was slowly decreased by decreasing the fuel flow rate. These instabilities were visually observed as an intermittent, large-amplitude "flapping" of the flame (see Fig. 13). During the flapping process, it appeared as though a large vortex, with a length scale comparable to the step height, was released. This flapping was evident in the measurements as "bursting" in the data signal (see Fig. 14). The time interval between these events decreased as equivalence ratio was decreased. As equivalence ratio was decreased

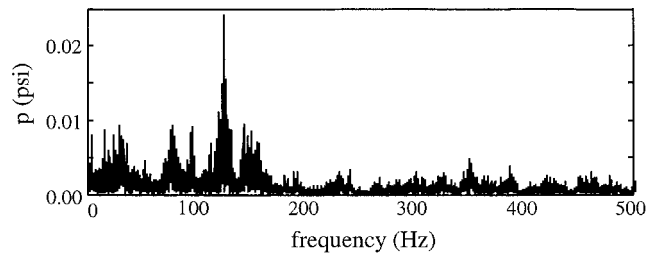

Fig. 12 Frequency spectrum of pressure fluctuation at $x = 67$ in. (170 cm) during stable combustion ($\phi = 0.83$).

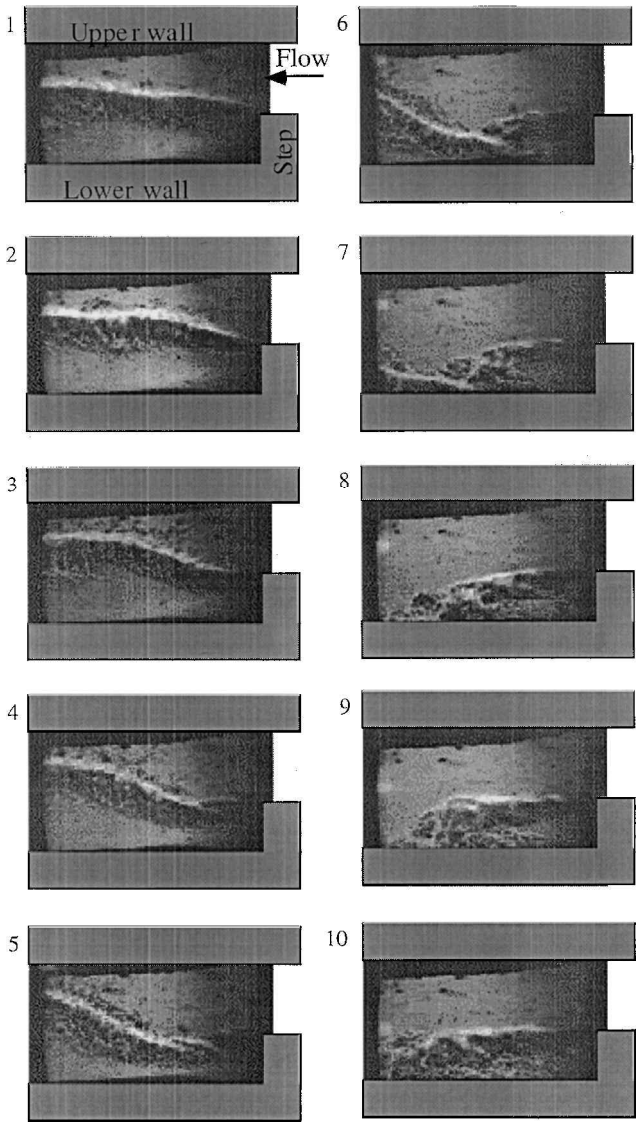

Fig. 13 Consecutive frames of shadowgraph film showing approximately $\frac{1}{2}$ cycle of 48-Hz flapping. Framing rate = 1050 frames/s; exposure time = 1.0 μs.

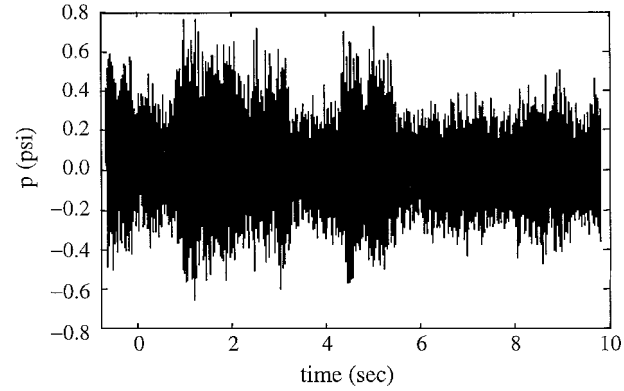

Fig. 14 Time history of pressure fluctuation at $x = 12.0$ in. (30.5 cm) showing bursting during unstable combustion; $\phi = 0.73$.

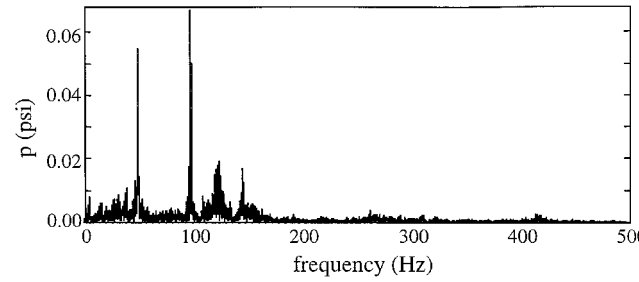

Fig. 15 Frequency spectrum of pressure fluctuation at $x = 67.0$ in. (170 cm) showing peaks at 48 and 96 Hz.

further, the increasing severity of the instability induced the global extinction of the combustor. The highest equivalence ratio at which the flame flapping phenomenon was observed was approximately 0.75. This corresponded to a stability limit, below which stable operation was not achieved. At higher airflow rates this value was slightly lower and was correspondingly higher at low airflow rates. The equivalence ratio at combustor blowout ranged from 0.63 to 0.67 and was also a mild function of airflow rate over the range of interest. These two observations are related, in that combustor blowout was often triggered by the unstable behavior. All results discussed in this section were for an airflow rate of 0.8 lbm/s (0.36 kg/s), which corresponded to a step approach velocity of 87 ft/s (26.5 m/s).

Spectral analysis of the data records during unstable combustion indicated large peaks at frequencies of 48 and 96 Hz, as shown in Fig. 15. This FFT analysis was performed for the entire data record. Further analysis of these data indicated that these two peaks represent the effects of the periodic flame flapping during the bursts. Figure 16 illustrates how the frequency of the dominant mode shifted from the stable 124-Hz mode in between the bursts to 96 Hz during the bursts. The first plot in this figure shows a time trace of the unstable combustor pressure. The second is representative of a sliding time-windowed FFT, showing the change in the spectral content of the signal with time as a contour plot. The third plot shows the change in the frequency (over the range of 75–200 Hz) of the dominant mode as a function of time.

The 96- and 48-Hz modes grew and decayed simultaneously. The acoustic wavelength of the 48-Hz mode corresponded roughly to a $\frac{1}{4}$-wave mode for the length between the venturi and the step. This corresponds well with the predicted mode shape shown in Fig. 7. It is likely that the 96-Hz signal represented a harmonic of the 48-Hz signal (an exact multiple). This behavior is not unusual in systems that are in a high-amplitude limit cycle. An alternative explanation is that the 96-Hz mode was a reflection of the 48-Hz signal between the step and the exit plane. Because the step lies at the midpoint of the entire rig, the frequency of the reflected wave was doubled to 96 from 48 Hz. The likelihood of this relationship between the two modes was assessed using the numerical technique described in the preceding section and cannot be completely discounted.

The shape of the 48-Hz mode (see Fig. 7) had a pressure node (velocity antinode) at the step, where the flame was stabilized. The shear layer formed at the trailing edge of the step (see Fig. 1) will be most sensitive at this location. This might explain the drastic shear-layer flapping action that resulted from the thermoacoustic coupling associated with this mode.

The combination of data from a number of tests at differing equivalence ratios enabled the examination of the onset of the instability as a function of equivalence ratio. In Fig. 17 the amplitudes of the 124-, 96-, and 48-Hz components are plotted vs equivalence ratio for one pressure sensor, located at 12.0 in. (30.5 cm) downstream of the step. As ϕ was decreased from a near-stoichiometric level, the magnitude of the 124-Hz oscillations grew steadily until approximately $\phi = 0.75$. At this point both the 48- and 96-Hz signals increased rapidly in magnitude, while the level of the 124-Hz signal dropped. This implies that the growth of the 124-Hz mode to a high level might have "triggered" a transition into the high-amplitude, low-frequency unstable behavior at this point. The 96- and 48-Hz signals were always present in the data but were often at a low level during stable combustion. Although a single pressure channel has been used to illustrate the behavior of this phenomenon, similar behavior was observed on the other measurements.

The high-speed shadowgraph films (frames of which are shown in Fig. 13) taken during unstable combustion indicated that the flame flapping which was evident during the unstable bursts occurred at

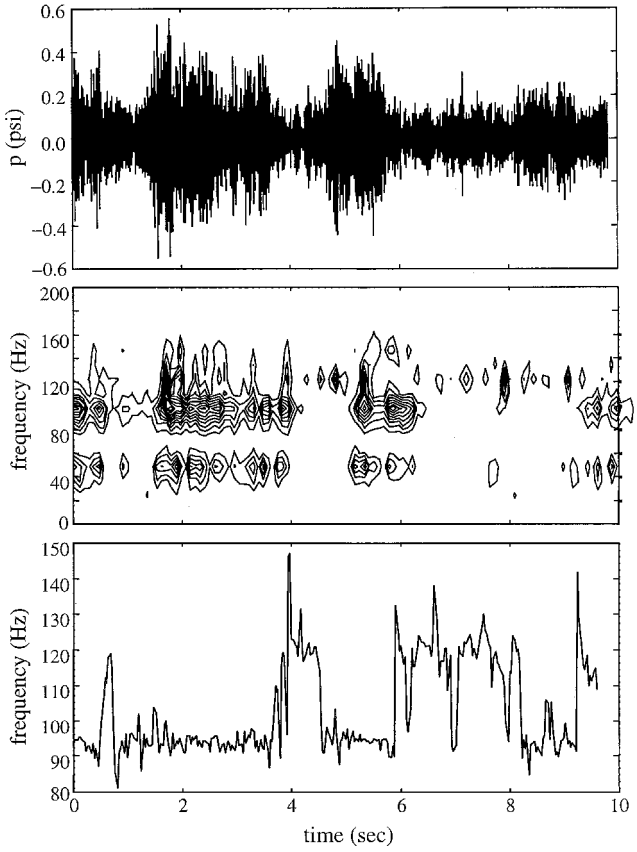

Fig. 16 Mode switching during bursting phenomenon in pressure measurement at $x = 67.0$ in. (170 cm). Unstable combustion; $\phi = 0.73$. Most energetic frequency filtered between 75–200 Hz (third plot only).

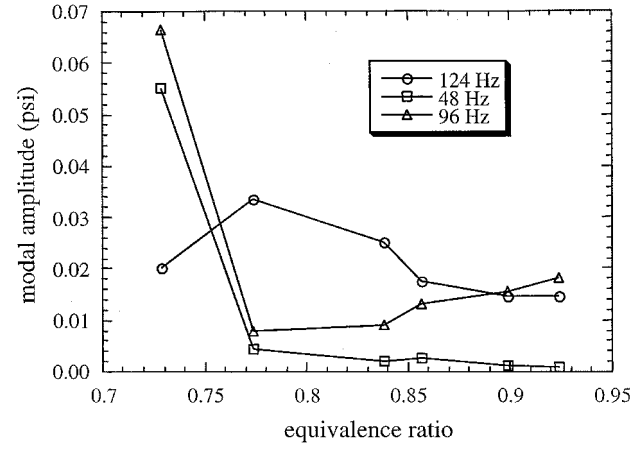

Fig. 17 Switching of most energetic modes with decreasing equivalence ratio.

a frequency of approximately 50 Hz, corresponding well with the 48-Hz peak in the data. A nondimensional examination of the different spectral modes observed in both stable and unstable combustion proved useful in comparing results from the current experiment and those obtained by others.[5,6] The 48- and 124-Hz modes correspond to Strouhal numbers of 0.05 and 0.12 [using $u_{\text{step}} = 87$ ft/s (26.5 m/s)], respectively.

As already indicated, other researchers have observed the same flame-flapping phenomenon observed in this experiment. In each case the flapping occurred at a frequency significantly lower than that of either the dominant duct acoustic mode or the shear-layer shedding process. In each case a large vortex was shed from behind the step. Najm and Ghoniem[4] refer to this phenomenon as a "wake mode" instability in order to distinguish it from the hydrodynamic shear-layer instability. They describe it as an inherent instability of the recirculation zone that occurs at Strouhal numbers of 0.05–0.2, based on step height. They also state that this phenomenon is consistent with the Rayleigh criterion, through which heat release and pressure fluctuations couple, leading to the growth of the instability. Although all three of the dominant modes observed in this experiment fall within this range, the 48-Hz mode fits the physical description best, as it corresponds with the flapping motion of the flame. Sterling[6] noted that flapping occurred at a subharmonic of the duct acoustic frequency. For the current experiment this should represent flapping at some integral fraction of a $\frac{3}{4}$-wave mode. The wavelength of the 48-Hz signal might have indicated a $\frac{1}{4}$-wave mode for the entire rig (not just the inlet; resolution of the mode shape downstream of the step was very coarse). In a system with varying cross-sectional area and thermoacoustic coupling, modal frequencies need not be integral multiples of one another, but harmonics and subharmonics are integral multiples of one another.

During the high-amplitude, low-frequency oscillations, it was determined that the effects of fuel system coupling could not be discounted. The amplitude of the 48-Hz pressure oscillations approached the magnitude of the pressure drop incurred by the fuel passing through the injection orifices. However, as already mentioned, the injection manifolds were isolated from the rest of the fuel delivery system by choked orifices so that the volume affected was minimal. In addition, the characteristic acoustic modes of the fuel injection manifold were estimated to occur at significantly higher frequencies than those observed in the instability.

Other investigators[13,14] have attributed instabilities in lean, premixed systems to fluctuations in equivalence ratio at the flame front. These fluctuations were driven by variations in airflow rate in response to acoustic pressure fluctuations. Lieuwen et al.[13] correlated the existence of this type of instability with the ratio of the convective timescale between the fuel injector and the flame front and the period of the acoustic oscillations. For this combustor the premixing section is rather long, leading to a convective time of approximately 45 ms. This results in a ratio of convective to acoustic timescales of approximately 2.2 for the 48-Hz mode. Most of the results in Lieuwen et al.[13] show that this ratio should be approximately one for instabilities to occur. Although this simple analysis is not sufficient to rule out equivalence ratio fluctuations as a driving force, it seems to indicate that the probability of this mechanism being dominant is low.

The low-frequency flame-flapping phenomenon is similar to that observed in experiments conducted at higher equivalence ratios, away from the lean blowout limit.[5,6] This experiment differed in that it was performed at leaner conditions and that the instability was triggered by decreasing the fuel flow to a leaner condition, whereas in the other experiments it was often triggered by increasing the fuel flow. This difference is interesting and can relate to the ratio of the characteristic combustion timescales to the acoustic timescale. The preferential driving of the 48-Hz mode at low equivalence ratios might be tied to increases in the characteristic combustion time τ with decreasing equivalence ratio. At higher values of ϕ, the value of τ is probably too short to excite the 48-Hz mode, but as the equivalence ratio was decreased τ increased[15] allowing thermoacoustic coupling to occur, through mechanisms similar to those explained by Lieuwen et al.[13]

Conclusions

An investigation was conducted in order to characterize the combustion instabilities that were observed in a lean, premixed step combustor at equivalence ratios approaching lean blowout. Experimentally, measurements of static wall pressure were acquired in addition to high-speed visualization of the reacting flowfield. These measurements were acquired under both unstable and stable combusting conditions. Numerically, an unsteady quasi-one-dimensional analysis was developed and applied to the backward-facing-step combustor rig. The analysis tool was used to identify the critical acoustic frequencies of the problem and agreed well with the dominant frequencies found in the experiment.

The results showed that, during stable combustion, the dominant duct acoustic mode, possibly coupled with the shear-layer vortex

shedding process, produced spectral components at 124 Hz in all of the measured variables. Combustion was stable at fuel/air equivalence ratios above 0.80, indicating that damping exceeded driving of the acoustic modes under those conditions. The analysis indicated that the strongest acoustic mode was found to be 127 Hz, comparing favorably with 124 Hz found in experiment. Weaker acoustic modes were predicted at 49, 234, and 386 Hz.

As the combustor equivalence ratio was decreased, the amplitude of the 124-Hz acoustic mode grew, until at approximately $\phi = 0.75$, large-amplitude, low-frequency oscillations were encountered. These oscillations were caused by the flapping of the flame as a large vortex was released from the region behind the step and occurred at 48 Hz. As the equivalence ratio was reduced further, the flapping became more violent, eventually causing the blowout of the combustor.

Numerically, a coupling of the heat release to the step velocity produced an unstable mode at the natural acoustic frequency of the combustor. The frequency of the unstable mode depended on characteristic time used in the model. The analysis complemented the experiment by providing insight into the physical mechanisms leading to the frequencies observed in the experiment. Forcing the system at the unstable frequency found in the experiment (48 Hz) produced a 96-Hz harmonic and the 127-Hz acoustic mode, as found in experiment.

The growth of the 124-Hz acoustic mode with the reduction in equivalence ratio appeared to trigger the low-frequency flame flapping. The flame flapping was attributed to coupling of the combustor heat release and acoustics with a wake mode instability, related to the unsteadiness of the recirculation zone behind the step.

For the one-dimensional analysis to be useful as a stand-alone simulation tool, models are needed to predict the correct characteristic timescales associated with the fluid-dynamic mixing and combustion. Critical for a simulation tool is the ability to capture the dependence of the instability on equivalence ratio that was observed in the experimental data. In the future it is planned to couple the one-dimensional analysis with a two-dimensional Navier–Stokes solver. This will be useful to investigate the coupling between the fluid-dynamic mixing and the acoustics of the system.

No previous documentation of these lean-limit combustion instabilities for the backward-facing-step configuration has been identified. This problem is not unique to this configuration, and the tools and understanding developed in this investigation will be valuable in examining and controlling more realistic systems.

Acknowledgments

This study was funded through the United Technologies Research Center core technology programs in Chemical Sciences and Active Combustion Control. The authors are grateful to William Proscia for his efforts in the development of the analyses and the planning of the experiment. The contributions of Gavin Hendricks to the development of the numerical procedures were greatly appreciated. Young Man Cho provided useful insight on the nature of the instabilities and valuable advice on digital signal processing techniques. The efforts of Torger Anderson, Walter Borst, Robert Haas, Randall Decker, and James Macleod in the conduct of the experiment were invaluable. The authors would also like to thank Danning You for improving the figure quality.

References

[1]Eaton, J. K., and Johnston, J. P., "A Review of Research on Subsonic Turbulent Flow Reattachment," AIAA Paper 80-1438, July 1980.

[2]Pitz, R. W., "An Experimental Study of Combustion: The Turbulent Structure of a Reacting Shear Layer Formed at a Rearward-Facing Step," Ph.D. Dissertation, Dept. of Mechanical Engineering, Univ. of California, Berkeley, 1981.

[3]Ganji, A. R., and Sawyer, R. F., "An Experimental Study of the Flowfield of a Two-Dimensional Premixed Turbulent Flame," *AIAA Journal*, Vol. 18, No. 7, 1980, pp. 817–824.

[4]Najm, H. N., and Ghoniem, A. F., "Coupling Between Vorticity and Pressure Oscillations in Combustion Instability," *Journal of Propulsion and Power*, Vol. 10, No. 6, 1994, pp. 769–776.

[5]Keller, J. O., Vaneveld, L., Korschelt, D., Ghoniem, A. F., Daily, J. W., and Oppenheim, A. K., "Mechanism of Instabilities in Turbulent Combustion Leading to Flashback," AIAA Paper 81-0107, Jan. 1981.

[6]Sterling, J. D., "Longitudinal Mode Combustion Instabilities in Air Breathing Engines," Ph.D. Dissertation, Dept. of Mechanical Engineering, California Inst. of Technology, Pasadena, 1987.

[7]Hautman, D. J., Haas, R. J., and Chiappetta, L., "Transverse Gaseous Injection into Subsonic Air Flows," AIAA Paper 91-0576, Jan. 1991.

[8]Holdeman, J. D., and Srinivasan, R., "Modeling Dilution Jet Flowfields," *Journal of Propulsion and Power*, Vol. 2, No. 1, 1986, pp. 4–10.

[9]Roe, P., "Approximate Riemann Solvers, Parameter Vectors and Difference Schemes," *Journal of Computational Physics*, Vol. 43, No. 2, 1981, pp. 357–372.

[10]Choi, D., "A Navier–Stokes Analysis of Film Cooling in a Turbine Blade," AIAA Paper 93-0158, Jan. 1993.

[11]Choi, D., and Knight, C. J., "Application of Scalar Implicit Approximate Factorization for an Underwater Magneto Hydrodynamic Propulsion System Analysis," *AIAA Journal*, Vol. 31, No. 2, 1993, pp. 286–293.

[12]Wake, B. E., and Choi, D., "Numerical Investigation of Higher-Order Upwinded Differencing for Vortex Convection," AIAA Paper 95-1719, June 1995.

[13]Lieuwen, T., Torres, H., Johnson, C., and Zinn, B. T., "A Mechanism of Combustion Instability in Lean Premixed Gas Turbine Combustors," American Society of Mechanical Engineers, Paper 99-GT-3, June 1999.

[14]Peracchio, A. A., and Proscia, W. M., "Nonlinear Heat-Release/Acoustic Model for Thermoacoustic Instability in Lean Premixed Combustors," American Society of Mechanical Engineers, Paper 98-GT-269, June 1998.

[15]Zukoski, E., and Oates, G. (eds.), *The Aerothermodynamics of Aircraft Gas Turbine Engines*, Air Force Propulsion Lab., Dayton, OH, 1978.